Research Article | Vol. 34, No. 8 / 20 Apr 2026 / Optics Express 14445

Optics EXPRESS

Small-signal system-level analysis of traveling-wave Mach-Zehnder modulators

TINUS PANNIER,* LUCAS VAN SEVEREN, MARIJN WERBROUCK, AND PETER OSSIEUR

IDLab, Dept. of Information Technology, Ghent University - imec, Technologiepark-Zwijnaarde 126, 9052 Ghent, Belgium

*tinus.pannier@ugent.be

Abstract: Mach-Zehnder modulators are widely used in high-speed optical communication systems due to their versatility and their ability to adopt a traveling-wave design to reach high modulation bandwidths. Existing analytical descriptions of these devices have focused on the derivation of a normalized amplitude frequency response, but a more comprehensive, detailed analysis has thus far been lacking. In this paper, we use a rigorous mathematical framework to present a small-signal system-level analysis of traveling-wave Mach-Zehnder modulators. Special attention has been paid to the interaction between the electrical and the optical domains, and electro-optical-electrical (EOE) S-parameters are formally derived. From this, modulator gain and bandwidth are discussed in depth, as well as velocity matching, and the importance of the electrical phase and group index. Additionally, minimum transmission point biasing for coherent systems is analyzed and compared against quadrature point biasing.

1. Introduction

External modulators are widely used in broadband optical communication systems because of their performance advantages over direct modulation of the laser source. Next to the electro-absorption modulator and the ring modulator, the Mach-Zehnder modulator (MZM) is a trusted option because of its high optical bandwidth, low chirp and straightforward extension to coherent modulation formats through the use of an IQ modulator. Since MZMs tend to be physically long devices, a traveling-wave topology has to be employed for high-speed operation. First described by Kaminow [1], a traveling-wave MZM (TWMZM) provides velocity matching between the electrical and optical waves to achieve broadband operation [2]. In the pursuit for higher data rates, modulation bandwidth has become a key performance metric.

In an optical modulator, an electrical signal is up-converted onto an optical carrier. Since the conversion is thus from the electrical domain (DC to ~ 100 GHz) to the optical domain (~ 200 THz), a description based on transfer functions, as is common in linear circuit analysis, is not directly possible. However, a transfer function, and its corresponding bandwidth, can be defined by implicitly assuming the optical signal is down-converted back to the electrical domain first by a suitable ideal optical receiver. The frequency response of the resulting linear electro-optical-electrical (EOE) channel is commonly referred to as the electro-optical (EO) modulation response or the EO S_{21} of the modulator. However, to make the down-conversion to the electrical domain explicit, these properties will be referred to as the EOE transfer function or the EOE S_{21} in this text. Using these observations as a starting point, a rigorous, small-signal, system-level description of TWMZMs was developed.

Existing frequency domain descriptions of TWMZMs mostly focus on the derivation of a qualitative performance indicator, often referred to as the modulation response [3], the modulation depth [4], the average voltage experienced by a photon [5–8], or the modulation reduction factor [8,9]. Although these models correctly predict the EOE normalized amplitude frequency response, additional insight can be gained from a system-level approach which provides a description of

#586920 https://doi.org/10.1364/OE.586920
Journal © 2026 Received 5 Dec 2025; revised 15 Jan 2026; accepted 30 Jan 2026; published 9 Apr 2026

all electrical and optical signals throughout the device. By analyzing the interaction between the electrical and optical domains, a formal expression for the EOE S_{21} is derived, and the modulator gain, bandwidth and group delay variations are discussed for various conditions. Velocity matching is analyzed in depth for both broadband and narrowband operation, and the importance of the optical group index, the electrical phase index and the electrical group index is clarified.

The term EOE S_{21} stems from the use of S-parameters to characterize electronic components using a vector network analyzer (VNA), and has proven to be the method of choice for high-speed frequency domain measurements. By incorporating a suitable photodetector in the measurement setup, modulators can be characterized by S-parameters as well, resulting in the so-called EOE S_{21} [10]. This parameter captures both the modulator frequency response and gain, and is therefore a good metric of modulator performance. However, in literature, the measured EOE S_{21} is often normalized and the gain is not discussed.

The following section starts with a short introduction on signal notations, after which the most fundamental equations governing traveling-wave modulator behavior are derived. These results are then applied to quadrature point biasing in Section 3, which in turn lays the groundwork for the formal introduction of EOE S-parameters in Section 4. Thereafter, an analysis of velocity matching, electrical losses and impedance mismatch is presented in Section 5. Section 6 applies the results of Section 2 to minimum transmission point biasing, after which Section 7 concludes the article. The appendix contains a table listing key symbols and their units.

2. Traveling-wave Mach-Zehnder modulator

2.1. Signal notations

Since performing calculations between the electrical and optical domains is sensitive to mathematical notations, it is important to carefully define the involved signals. An optical signal consists of three electric and three magnetic field components. To make the analysis manageable, we only consider signals propagating in a single-mode waveguide, which can be described by a single scalar component. The optical field $\hat{e}(t)$, which is a real-valued band-pass signal around f_0 (with $f_0 = 193\,\text{THz}$ for communication in the C-band for example), can be represented by its complex envelope $e(t)$ as

$$\hat{e}(t) = \sqrt{2}\,\Re\{e(t)\,e^{j2\pi f_0 t}\} \tag{1}$$

The complex envelope $e(t)$ is a complex-valued low-pass signal, with a signal bandwidth $B \ll f_0$. In the frequency domain, this relation can be written as

$$\hat{E}(f) = \frac{\sqrt{2}}{2}E(f-f_0) + \frac{\sqrt{2}}{2}E^*(-f-f_0) \tag{2}$$

where * denotes the complex conjugate. The spectra $E(f)$ and $\hat{E}(f)$ are given by the continuous time Fourier Transform (CTFT) of the signals $e(t)$, respectively $\hat{e}(t)$:

$$E(f) = \int_{-\infty}^{\infty} e(t)\,e^{-j2\pi ft}\,\mathrm{d}t \tag{3}$$

$$\hat{E}(f) = \int_{-\infty}^{\infty} \hat{e}(t)\,e^{-j2\pi ft}\,\mathrm{d}t \tag{4}$$

This relationship is illustrated in Fig. 1.

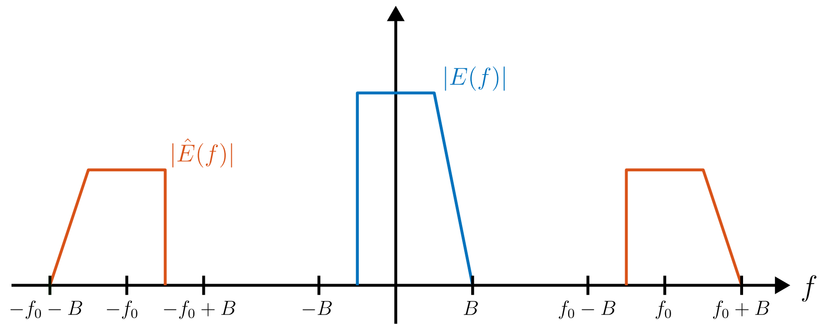

Fig. 1. Illustration of the relationship between the real-valued band-pass signal $\hat{e}(t)$ and its complex envelope $e(t)$.

2.2. Traveling-wave phase modulator

Propagation through an optical single-mode waveguide can in general be described by the propagation factor β, which can be expanded around $\omega = 2\pi f = 0$ as

$$\beta(\omega) = \beta_0 + \beta_1\omega + \frac{1}{2}\beta_2\omega^2 + \frac{1}{6}\beta_3\omega^3 + \cdots \tag{5}$$

with

$$\beta_m = \left.\frac{\mathrm{d}^m\beta}{\mathrm{d}^m\omega}\right|_0 \tag{6}$$

The coefficient β_0 introduces a phase shift, β_1 is related to the group delay, and β_2 is called the group velocity dispersion (GVD) parameter [11]. Propagation over length $\mathcal{L}$ of the signal $e_{in}(t)$ through a medium with propagation factor $\beta(\omega)$ is described in complex envelope notation by the linear time-invariant (LTI) filter $H(f) = e^{-j\beta(2\pi f)\mathcal{L}}$, such that

$$e_{out}(t) = \int_{-\infty}^{\infty} E_{in}(f)\, e^{-j\beta(2\pi f)\mathcal{L}}\, e^{j2\pi ft}\, \mathrm{d}f \tag{7}$$

An ideal phase modulator induces a phase shift onto the optical signal $e_{in}(t)$, proportional to the applied voltage V:

$$e_{out}(t) = e^{-j\pi\frac{V}{V_\pi}}\, e_{in}(t) \tag{8}$$

In practice, every phase modulator has a finite efficiency, described by the constant product $V_\pi\mathcal{L}$. This implies that the modulator has to be sufficiently long, in order for V_π to be within the voltage range of the current generation driver amplifiers. However, if the modulator becomes *electrically* long, (8) no longer holds, because the propagation delay of the electrical and optical signals was not taken into consideration. To account for these propagation effects, the phase modulator has to be modeled as an electrical transmission line, through which the optical signal propagates according to a voltage-dependent propagation factor β.

The situation is presented in Fig. 2. A transmission line runs from $z = 0$ to $z = \mathcal{L}$. Along this transmission line, a voltage $v(z, t)$ is present. The transmission line is divided into N sections of length Δz, such that $N\Delta z = \mathcal{L}$. The voltage $v(z, t)$ is assumed to be constant over Δz, i.e. Δz is electrically short, such that

$$v(z, t) = v_i(t),\ z \in (i\Delta z, (i+1)\Delta z),\ i = 0, .., N-1 \tag{9}$$

The optical signal, represented by its complex envelope $e_{in}(t)$, enters the optical waveguide that runs along the transmission line at $z = 0$. The optical signal exiting the waveguide at $z = \mathcal{L}$

is denoted as $e_{out}(t)$. The waveguide consists of an ideal phase modulator, with the phase being controlled by the voltage $v(z,t)$ that runs along it on the transmission line. The propagation factor (see (5)) of section i is given by

$$\beta_i(f;t) = \beta_{0,i}(t) + \beta_{1,i}\, 2\pi f \tag{10}$$

$$= \frac{2\pi}{\lambda_0}\,(n_0 + \Delta n_i(t)) + \tau 2\pi f \tag{11}$$

with n_0 the effective index of the propagating mode and τ the group delay per unit length [12], which is assumed to be constant, regardless of the applied voltage. Dispersion in the optical waveguide is neglected: there are no quadratic or higher order terms included in (10). This assumption can be justified by the mm-scale length of optical modulators, combined with the dispersion levels of common integrated waveguides, which typically do not exceed those of standard single-mode fiber (around 20 ps/(km · nm) in C-band [11]) by more than three orders of magnitude [13–15]. The induced change to the effective index $\Delta n_i(t)$ is given by

$$\Delta n_i(t) = \frac{\lambda_0}{2V_\pi \mathcal{L}}\, v_i(t) \tag{12}$$

with $V_\pi \mathcal{L}$ the phase modulator efficiency, and λ_0 the optical wavelength in vacuum. Every section i acts as a linear time-varying (LTV) filter $H_i(f;t) = e^{-j\beta_i(f;t)\Delta z}$ on the optical wave:

$$e_{out,i}(t) = \int_{-\infty}^{\infty} E_{in,i}(f)\, e^{-j\beta_i(f;t)\Delta z}\, e^{j2\pi f t}\, \mathrm{d}f \tag{13}$$

$$= e^{-j\beta_{0,i}(t)\Delta z}\, e_{in,i}(t - \tau\Delta z) \tag{14}$$

We can now calculate the cascade of LTV filters $H_i(f;t)$ for $i = 0, .., N-1$. Considering that $e_{out,i}(t) = e_{in,i+1}(t)$, $e_{in}(t) = e_{in,0}(t)$ and $e_{out,N-1}(t) = e_{out}(t)$, we get

$$e_{out,0}(t) = e^{-j\beta_{0,0}(t)\Delta z}\, e_{in}(t - \tau\Delta z) \tag{15}$$

$$e_{out,1}(t) = e^{-j\beta_{0,1}(t)\Delta z}\, e^{-j\beta_{0,0}(t-\tau\Delta z)\Delta z}\, e_{in}(t - 2\tau\Delta z) \tag{16}$$

$$e_{out,2}(t) = e^{-j\beta_{0,2}(t)\Delta z}\, e^{-j\beta_{0,1}(t-\tau\Delta z)\Delta z}\, e^{-j\beta_{0,0}(t-2\tau\Delta z)\Delta z}\, e_{in}(t - 3\tau\Delta z) \tag{17}$$

$$\vdots$$

$$e_{out}(t) = \prod_{i=0}^{N-1} e^{-j\beta_{0,i}\,(t-(N-1-i)\tau\Delta z)\Delta z}\, e_{in}(t - N\tau\Delta z) \tag{18}$$

This can be rewritten as

$$e_{out}(t) = \exp\left\{-j\frac{\pi}{V_\pi \mathcal{L}} \sum_{i=0}^{N-1} v_i\,(t - (N-1-i)\,\tau\Delta z)\,\Delta z\right\}\, e^{-j\frac{2\pi}{\lambda_0} n_0 \mathcal{L}}\, e_{in}(t - \tau\mathcal{L}) \tag{19}$$

If we take the limit for $\Delta z \to 0$ (or equivalently, $N \to \infty$), we get

$$e_{out}(t) = \exp\left\{-j\frac{\pi}{V_\pi \mathcal{L}} \int_0^{\mathcal{L}} v(z, t + \tau(z - \mathcal{L}))\, \mathrm{d}z\right\}\, e^{-j\frac{2\pi}{\lambda_0} n_0 \mathcal{L}}\, e_{in}(t - \tau\mathcal{L}) \tag{20}$$

Indeed, in the simple case that $v(z,t) = V_0$, (20) reduces to

$$e_{out}(t) = e^{-j\pi\frac{V_0}{V_\pi}}\, e^{-j\frac{2\pi}{\lambda_0} n_0 \mathcal{L}}\, e_{in}(t - \tau\mathcal{L}) \tag{21}$$

which is precisely the result we expect: the first factor is the induced phase shift, the second factor is the phase shift corresponding to the path length, and the signal envelope is delayed by the group delay $\tau\mathcal{L}$.

Optics EXPRESS

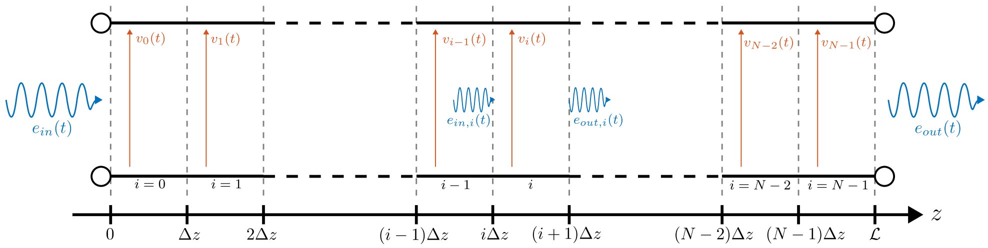

Fig. 2. Illustration of a traveling-wave phase modulator.

2.3. Optical losses

Up to this point, optical losses in the waveguide were neglected. If losses are assumed to be constant over the optical frequency range of interest, and not affected by the applied voltage $v(z,t)$, they can be included by simply adding the factor $e^{-\frac{\alpha}{2}\mathcal{L}}$ to (20), such that

$$|e_{out}(t)|^2 = e^{-\alpha\mathcal{L}}\,|e_{in}(t-\tau\mathcal{L})|^2 \tag{22}$$

In this equation, the attenuation coefficient α is expressed in units of [1/m]. In practice, attenuation is often reported in units of [dB/m]. Both quantities are related as

$$\alpha[\mathrm{dB/m}] \approx 4.343\,\alpha[1/\mathrm{m}] \tag{23}$$

2.4. Mach-Zehnder modulator

A TWMZM of length $\mathcal{L}$ is shown in Fig. 3. It consists of two lossless, uncoupled transmission lines with electrical propagation factor β_e and constant real-valued characteristic impedance Z_c. The optical phase shifter efficiency and loss are represented by $V_\pi\mathcal{L}$ and α, respectively. The optical input signal $e_{in}(t)$ is equally split into the two traveling-wave phase modulators, after which the lower branch experiences an additional phase shift of ϕ_B, before recombining again to obtain $e_{out}(t)$. The upper and lower branches of the modulator are controlled by the voltages $v_U(z,t)$, respectively $v_L(z,t)$. Based on (20), $e_{out}(t)$ can directly be determined as

$$\begin{aligned} e_{out}(t) = \frac{1}{2}\Bigg[&\exp\left\{-j\frac{\pi}{V_\pi\mathcal{L}}\int_0^{\mathcal{L}} v_U(z,t+\tau(z-\mathcal{L}))\,\mathrm{d}z\right\} \\ &+ e^{j\phi_B}\exp\left\{-j\frac{\pi}{V_\pi\mathcal{L}}\int_0^{\mathcal{L}} v_L(z,t+\tau(z-\mathcal{L}))\,\mathrm{d}z\right\}\Bigg] \\ &e^{-\frac{\alpha}{2}\mathcal{L}}\,e^{-j\frac{2\pi}{\lambda_0}n_0\mathcal{L}}\,e_{in}(t-\tau\mathcal{L}) \end{aligned} \tag{24}$$

The factor $1/2$ in (24) stems from splitting and recombining the optical signal. The phase shift ϕ_B is used to bias the modulator in either quadrature point (QP) or minimum transmission point (MTP). The biasing of the modulator is important, since not all bias points result in a linear EOE channel after down-conversion to the electrical domain by a chosen ideal optical receiver. In this analysis, two linear EOE channels are discussed. QP biasing with direct detection is discussed hereafter, whereas MTP biasing with homodyne coherent detection is covered in Section 6. Other modulator structures, such as advanced, non-uniform designs, can often be partitioned into multiple phase shifter or waveguide segments. Each segment could then be described by (20) or (7), after which the overall response is found by cascading all segments. Examples of such segmented designs include slow-wave electrode designs [16], electro-optic equalizers [17], and modulators with integrated segmented drivers [18].

Optics EXPRESS

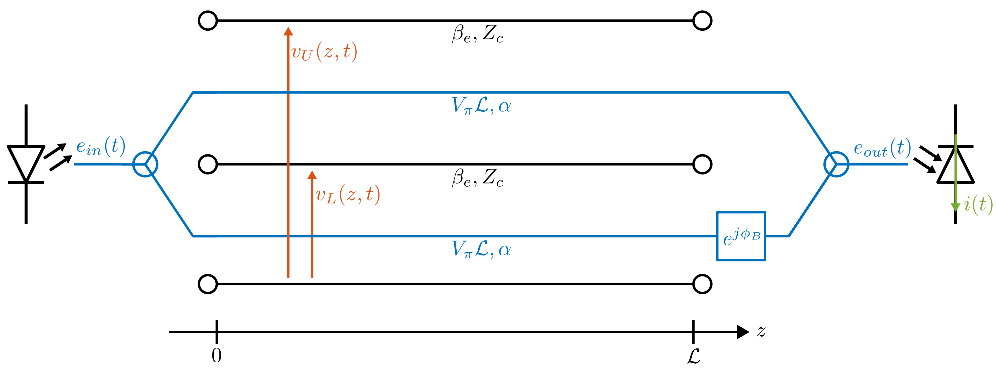

Fig. 3. Traveling-wave Mach-Zehnder modulator with direct detection.

3. Quadrature point biasing

For QP biasing, $\phi_B = -\frac{\pi}{2}$ or $e^{j\phi_B} = -j$ is chosen. Furthermore, if differential signaling (sometimes also referred to as push-pull) is used, $v_U(z,t) = -v_L(z,t) = \frac{1}{2}\, v_d(z,t)$, and (24) reduces to

$$\begin{aligned} e_{out}(t) = & e^{-j\frac{\pi}{4}} \cos\left\{\frac{\pi}{2V_\pi \mathcal{L}} \int_0^{\mathcal{L}} v_d(z, t + \tau(z - \mathcal{L}))\, \mathrm{d}z - \frac{\pi}{4}\right\} \\ & e^{-\frac{\alpha}{2}\mathcal{L}}\, e^{-j\frac{2\pi}{\lambda_0} n_0 \mathcal{L}}\, e_{in}(t - \tau\mathcal{L}) \end{aligned} \tag{25}$$

In the case of direct detection, the optical signal $e_{out}(t)$ is detected by a photodetector, as indicated in Fig. 3. The generated current $i(t)$ is linearly proportional to the magnitude squared of the complex envelope of the optical signal, such that

$$i(t) = R\,|e_{out}(t)|^2 \tag{26}$$

with the constant R the responsivity of the photodetector. The optical input signal $e_{in}(t)$ is coming directly from an ideal laser source with power P_s and frequency f_0. The signal phase was chosen arbitrarily to ease notations, such that

$$e_{in}(t) = \sqrt{P_s}\, e^{j\frac{2\pi}{\lambda_0} n_0 \mathcal{L}}\, e^{j\frac{\pi}{4}} \tag{27}$$

Substituting (27) and (25) into (26), we find

$$i(t) = RP_s\, e^{-\alpha\mathcal{L}} \cos^2\left\{\frac{\pi}{2V_\pi \mathcal{L}} \int_0^{\mathcal{L}} v_d(z, t + \tau(z - \mathcal{L}))\, \mathrm{d}z - \frac{\pi}{4}\right\} \tag{28}$$

We will limit the analysis to a small-signal analysis which is only valid for $|v_d| \ll V_\pi$. To this end, (28) can be linearized around $v_d = 0$. Since $\cos^2(x - \frac{\pi}{4}) \approx \frac{1}{2} + x$ for small x, $i(t)$ can be approximated as

$$i(t) \approx \underbrace{\frac{RP_s e^{-\alpha\mathcal{L}}}{2}}_{\mathrm{DC}} + \underbrace{\frac{RP_s \pi}{2V_\pi \mathcal{L}}\, e^{-\alpha\mathcal{L}} \int_0^{\mathcal{L}} v_d(z, t + \tau(z - \mathcal{L}))\, \mathrm{d}z}_{\Delta i(t)} \tag{29}$$

The first term in this expression corresponds to the DC photocurrent, where the factor $1/2$ is introduced by the QP biasing. The second term $\Delta i(t)$ is the output signal of the EOE channel and will be the focus of the remainder of the analysis.

3.1. EOE transfer function

Before determining the transfer function between the input signal $v_d(z, t)$ and the output signal $\Delta i(t)$ in (29), it has to be observed that this relationship is indeed linear, and as such a transfer function can be defined. If we limit the discussion to sinusoidal signals, the time-domain signals $v_d(z, t)$ and $\Delta i(t)$ can be represented by their complex phasors $V_d(z)$, respectively I, as

$$v_d(z, t) = \Re\{V_d(z)e^{j\omega_m t}\} \tag{30}$$

$$\Delta i(t) = \Re\{Ie^{j\omega_m t}\} \tag{31}$$

with $f_m = \frac{\omega_m}{2\pi}$ the modulation frequency. To find the phasor representation of $v_d(z, t + \tau(z - \mathcal{L}))$, it can be written as

$$v_d(z, t + \tau(z - \mathcal{L})) = \Re\left\{V_d(z)\, e^{j\omega_m(t+\tau(z-\mathcal{L}))}\right\} \tag{32}$$

from which the phasor representation $V_d(z)\, e^{j\omega_m \tau(z-\mathcal{L})}$ can be found by identification. By transforming $\Delta i(t)$ in (29) to the phasor domain, we finally get

$$I = \frac{RP_s\pi}{2V_\pi\mathcal{L}}\, e^{-\alpha\mathcal{L}}\, e^{-j\omega_m\tau\mathcal{L}} \int_0^{\mathcal{L}} V_d(z)\, e^{j\omega_m\tau z}\, \mathrm{d}z \tag{33}$$

This equation is the EOE transfer function of a TWMZM for QP biasing and direct detection, and gives valuable insight into its functioning. The frequency response is determined by the voltage distribution $V_d(z)$, and how it interacts, on average over the length of the modulator, with the optical signal propagating with group velocity $1/\tau$. For a lossless transmission line at low frequency, $V_d(z) \approx V_d(0)$, and the DC gain is given by

$$\frac{I}{V_d(0)} = \frac{RP_s\pi}{2V_\pi\mathcal{L}}\,\mathcal{L}e^{-\alpha\mathcal{L}} \tag{34}$$

By varying the length $\mathcal{L}$, a trade-off exists between decreasing V_π or decreasing optical losses. This trade-off is captured by the factor $\mathcal{L}e^{-\alpha\mathcal{L}}$, and can be maximized by choosing $\mathcal{L} = \mathcal{L}_{\text{max, QP}}$, with

$$\mathcal{L}_{\text{max, QP}} = \frac{1}{\alpha} \tag{35}$$

The maximum modulator gain is then

$$\frac{I}{V_d(0)} = \frac{RP_s\pi}{2e}\,\frac{1}{V_\pi\mathcal{L}\alpha} \tag{36}$$

The product $V_\pi\mathcal{L}\alpha$ is a technology constant and is often used as figure of merit (FoM) to compare modulator phase shifters [19]. The factor RP_s is somewhat artificial, and is a consequence of the construction of the EOE channel.

3.2. Note on the definition of modulation bandwidth

The electrical modulation bandwidth of the EOE transfer function (33) is defined as the frequency $f_m = f_{3\,\text{dB}}$ for which I has decreased by 3 dB:

$$20\log_{10}\left|\frac{I(f_{3\,\text{dB}})}{I(0)}\right| = -3\,\text{dB} \tag{37}$$

However, since I is originally a photocurrent, some authors [3,5,7] choose a $10\log_{10}$ definition, such that the modulation bandwidth is found by solving

$$10\log_{10}\left|\frac{I(f_{3\,\text{dB}})}{I(0)}\right| = -3\,\text{dB} \tag{38}$$

If the modulation bandwidth is used to convey an impression on the achievable data rates over the EOE channel, in the implicit understanding that a symbol rate R_s requires $f_{3\,\text{dB}} > R_s/2$, the

$20\log_{10}$ definition (37) should be used. Confusingly, the $10\log_{10}$ definition (38) results in bigger numbers for the modulation bandwidth, and should therefore be avoided. For consistency with systems definitions, we use the $20\log_{10}$ definition (37) throughout this text [10,20].

3.3. Optical spectrum

The output of the modulator can also be observed in the optical domain using an optical spectrum analyzer (OSA). To calculate the power spectral density (PSD) in the optical domain, we start from (25), and after linearization around $v_d = 0$, considering $\cos(x - \frac{\pi}{4}) \approx \frac{1}{\sqrt{2}}(1 + x)$, we find

$$e_{out}(t) = \frac{\sqrt{P_s}}{\sqrt{2}} e^{-\frac{\alpha}{2}\mathcal{L}} + \frac{\sqrt{P_s}\pi}{2\sqrt{2}\,V_\pi \mathcal{L}} e^{-\frac{\alpha}{2}\mathcal{L}} \int_0^{\mathcal{L}} v_d(z, t + \tau(z - \mathcal{L}))\,\mathrm{d}z \tag{39}$$

The PSD $S_{out}(f)$ is defined as the CTFT of the autocorrelation function of $e_{out}(t)$, i.e.

$$S_{out}(f) = \int_{-\infty}^{\infty} \langle e_{out}(t+u)e^*_{out}(t)\rangle_t \, e^{-j2\pi f u}\,\mathrm{d}u \tag{40}$$

where $\langle\cdot\rangle_t$ denotes the average over time t. If we limit the discussion again to sinusoidal signals, as in (30), we find

$$\begin{aligned} S_{out}(f) = {} & \frac{P_s}{2} e^{-\alpha\mathcal{L}}\,\delta(f) \\ & + \frac{P_s\pi^2}{32(V_\pi\mathcal{L})^2} e^{-\alpha\mathcal{L}} \left| \int_0^{\mathcal{L}} V_d(z)\, e^{j\omega_m \tau z}\,\mathrm{d}z \right|^2 \left(\delta(f - f_m) + \delta(f + f_m)\right) \end{aligned} \tag{41}$$

with $\delta(\cdot)$ the Dirac delta function. The PSD $\hat{S}_{out}(f)$ of the real-valued band-pass signal $\hat{e}_{out}(t)$ (see (1)) is then given by

$$\hat{S}_{out}(f) = \frac{1}{2}\left(S_{out}(f - f_0) + S_{out}(-f - f_0)\right) \tag{42}$$

The optical spectrum has components at f_0 and $f_0 \pm f_m$. Of particular interest is the magnitude of the components at $f_0 \pm f_m$, since these carry the same amplitude frequency response information as the EOE transfer function from (33). This result can be used to characterize modulators beyond the bandwidth of available lightwave component analyzers (LCAs) or VNAs [21].

4. EOE S-parameters

To further analyze (33), we need to solve the electrical problem first by determining $V_d(z)$. The equivalent circuit of the EOE channel is presented in Fig. 4. The modulator consists of two lossy, uncoupled transmission lines, running along the z-axis, with real-valued characteristic impedance Z_c and complex propagation factor γ_e [22], given by

$$\gamma_e(\omega_m) = \alpha_e(\omega_m) + j\beta_e(\omega_m) \tag{43}$$

where $\alpha_e(\omega_m)$ is the electrical loss coefficient and $\beta_e(\omega_m)$ the electrical propagation factor. Both transmission lines are terminated by the same termination resistor R_T. A generator E_g with output resistance R_{01} is connected via an ideal balun to drive the modulator in push-pull. There is no excitation at the common mode port, instead it is terminated by R_{03}. The photodetector is modeled by the parallel connection of the current source I (with I given by (33)) and the impedance Z_{PD}. The loading of subsequent receiver circuits is represented by R_{02}.

Since the modulator circuit is symmetrical and the common mode is not excited, we see that $V_U(z) = -V_L(z)$ and $I_U(z) = -I_L(z)$. From transmission line theory [22], it is known that a general

Optics EXPRESS

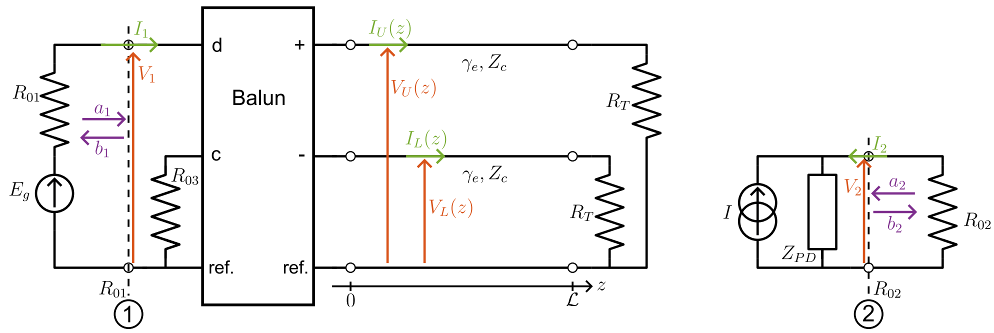

Fig. 4. Equivalent circuit of the EOE channel. The optical channel is not shown for readability.

solution of $V_U(z)$, $I_U(z)$, $V_L(z)$ and $I_L(z)$ can be written as the superposition of a forward and backward traveling wave:

$$V_U(z) = -V_L(z) = \frac{E_g}{2}[A^+ e^{-\gamma_e z} + A^- e^{\gamma_e z}] \tag{44}$$

$$I_U(z) = -I_L(z) = \frac{E_g}{2Z_c}[A^+ e^{-\gamma_e z} - A^- e^{\gamma_e z}] \tag{45}$$

The balun imposes the following relations onto the circuit:

$$V_1 = V_U(0) - V_L(0) \tag{46}$$

$$I_1 = \frac{1}{2}(I_U(0) - I_L(0)) \tag{47}$$

The generator voltage E_g is related to V_1 and I_1 as

$$E_g - R_{01} I_1 = V_1 \tag{48}$$

Finally, at $z = \mathcal{L}$, the termination resistor R_T determines that

$$V_U(\mathcal{L}) = R_T\, I_U(\mathcal{L}) \qquad V_L(\mathcal{L}) = R_T\, I_L(\mathcal{L}) \tag{49}$$

Solving the above equations for A^+ and A^-, we find

$$V_d(z) = V_U(z) - V_L(z) = E_g[A^+ e^{-\gamma_e z} + A^- e^{\gamma_e z}] \tag{50}$$

with

$$A^+ = \frac{1}{2}\,\frac{1 - K_S}{1 - K_S K_T e^{-2\gamma_e \mathcal{L}}} \qquad A^- = A^+ K_T e^{-2\gamma_e \mathcal{L}} \tag{51}$$

and

$$K_S = \frac{\frac{R_{01}}{2} - Z_c}{\frac{R_{01}}{2} + Z_c} \qquad K_T = \frac{R_T - Z_c}{R_T + Z_c} \tag{52}$$

If we consider the case $K_S = K_T = 0$ (no reflections), from (50) it follows that the voltage transfer function from $z = 0$ to $z = \mathcal{L}$ is given by

$$\left|\frac{V_d(\mathcal{L})}{V_d(0)}\right| = e^{-\alpha_e(\omega_m)\mathcal{L}} \tag{53}$$

This result coincides with the electrical transmission parameter $|S_{21}^{EE}|$ of the transmission line, when the S-parameter normalization impedances are chosen equal to Z_c.

Optics EXPRESS

To come to an EOE S-parameter description of the circuit in Fig. 4, we define two ports with real-valued reference impedances R_{01} and R_{02}. The scattering variables a_i and b_i are defined as

$$a_i = \frac{V_i + R_{0i} I_i}{2\sqrt{R_{0i}}} \qquad b_i = \frac{V_i - R_{0i} I_i}{2\sqrt{R_{0i}}} \tag{54}$$

with $i = 1, 2$. The scattering variables are related through the S-parameters as

$$b_1 = S_{11}^{EOE} a_1 + S_{12}^{EOE} a_2 \tag{55}$$

$$b_2 = S_{21}^{EOE} a_1 + S_{22}^{EOE} a_2 \tag{56}$$

Since port 2 is not excited in Fig. 4, $a_2 = 0$, and S_{21}^{EOE} is given by

$$S_{21}^{EOE} = \frac{b_2}{a_1} \tag{57}$$

It can be shown that

$$b_2 = \sqrt{R_{02}}\, \frac{Z_{PD}}{R_{02} + Z_{PD}} I \qquad a_1 = \frac{E_g}{2\sqrt{R_{01}}} \tag{58}$$

which eventually leads to

$$S_{21}^{EOE} = \sqrt{R_{01}R_{02}}\, \frac{Z_{PD}}{R_{02} + Z_{PD}} \frac{RP_s \pi}{V_\pi \mathcal{L}} e^{-\alpha \mathcal{L}} e^{-j\omega_m \tau \mathcal{L}} \int_0^{\mathcal{L}} [A^+ e^{-\gamma_e z} + A^- e^{\gamma_e z}]\, e^{j\omega_m \tau z}\, \mathrm{d}z \tag{59}$$

The other S-parameters can readily be determined as

$$S_{11}^{EOE} = \frac{Z_{in,d} - R_{01}}{Z_{in,d} + R_{01}} \tag{60}$$

$$S_{12}^{EOE} = 0 \tag{61}$$

$$S_{22}^{EOE} = \frac{Z_{PD} - R_{02}}{Z_{PD} + R_{02}} \tag{62}$$

with

$$Z_{in,d} = 2Z_c \frac{1 + K_T e^{-2\gamma_e \mathcal{L}}}{1 - K_T e^{-2\gamma_e \mathcal{L}}} \tag{63}$$

5. Analysis of the EOE S21

Before we delve into the high-frequency behavior of S_{21}^{EOE}, we first consider the gain at DC. Assuming $\gamma_e(0) \approx 0$, from (59) we find

$$|S_{21}^{EOE}(0)| = \sqrt{R_{01}R_{02}} \left| \frac{Z_{PD}}{R_{02} + Z_{PD}} \right| \frac{R_T}{\frac{R_{01}}{2} + R_T} \frac{RP_s \pi}{V_\pi \mathcal{L}} \mathcal{L} e^{-\alpha \mathcal{L}} \tag{64}$$

The modulator gain can be increased by choosing $\mathcal{L} = \mathcal{L}_{\text{max, QP}}$ (see (35)) or by increasing the termination resistor R_T. The dependence on Z_{PD} and the factor RP_s is somewhat artificial, and is a consequence of the construction of the EOE channel. The proportionality to $\sqrt{R_{01}R_{02}}$ is a result of the voltage controlled current source behavior of the equivalent circuit in Fig. 4.

Other than at DC, the complete result (59) for S_{21}^{EOE} is rather complicated to discuss, because it combines the three phenomena governing modulator high-frequency behavior: velocity matching, impedance mismatch and electrical losses [3]. Nevertheless, insight can be gained from analyzing these effects individually, after which they can be combined numerically through (59).

Optics EXPRESS

5.1. Velocity matching

To isolate the effect of electrical and optical signals propagating with different velocities along the modulator, we limit the discussion to $K_S = K_T = 0$ (no reflections) and choose $Z_{PD} = R_{02}$. From (59) we now find

$$S_{21}^{EOE}(\omega_m) = \frac{\sqrt{R_{01}R_{02}}}{4} \frac{RP_s\pi}{V_\pi \mathcal{L}} e^{-\alpha\mathcal{L}}\, e^{-j\omega_m\tau\mathcal{L}} \int_0^{\mathcal{L}} e^{-\alpha_e z}\, e^{j(\omega_m\tau-\beta_e)z}\,\mathrm{d}z \tag{65}$$

To ease notations, the dependence of α_e and β_e on ω_m was suppressed. If we further neglect the electrical attenuation on the transmission line by setting $\alpha_e = 0$, the above result simplifies to

$$S_{21}^{EOE}(\omega_m) = \frac{\sqrt{R_{01}R_{02}}}{4} \frac{RP_s\pi}{V_\pi \mathcal{L}} \mathcal{L}e^{-\alpha\mathcal{L}} \exp\left(-j\frac{\omega_m\tau+\beta_e}{2}\mathcal{L}\right) \operatorname{sinc}\left(\frac{\omega_m\tau-\beta_e}{2}\mathcal{L}\right) \tag{66}$$

with $\operatorname{sinc}(x) = \sin(x)/x$.

Under the aforementioned conditions, S_{21}^{EOE} now follows a sinc$(\cdot)$ behavior, and its bandwidth is therefore limited as such, unless the argument of the sinc$(\cdot)$ can be made identically zero, i.e.

$$\beta_e(\omega_m) = \omega_m\tau, \quad \forall\omega_m \tag{67}$$

The optical group delay per unit length τ can be written as

$$\tau = \frac{n_{og}}{c} \tag{68}$$

with n_{og} the optical group index. The condition in (67) now becomes

$$\beta_e(\omega_m) = \frac{\omega_m}{c} n_{og}, \quad \forall\omega_m \tag{69}$$

To meet this condition, a transmission line should have no dispersion, i.e. β_e is a linear function of ω_m and can therefore be written as

$$\beta_e(\omega_m) = \frac{\omega_m}{c} n_e \tag{70}$$

where the constant n_e is the electrical phase index. Additionally, the electrical phase index n_e should match the optical group index:

$$n_e = n_{og} \tag{71}$$

These conditions are known as the velocity matching conditions for a traveling-wave Mach-Zehnder modulator. In practice, however, these conditions are not always achievable. This can be due to dispersion in the transmission line, or because the electrical phase index n_e cannot be matched to the optical group index n_{og}. The following paragraphs discuss these two limiting factors in more detail.

Transmission line without dispersion. If the transmission line is dispersionless, as is the case for an ideal lossless transverse electromagnetic (TEM) transmission line [22], β_e can be written as (70) and S_{21}^{EOE} becomes

$$S_{21}^{EOE}(\omega_m) = \frac{\sqrt{R_{01}R_{02}}}{4} \frac{RP_s\pi}{V_\pi \mathcal{L}} \mathcal{L}e^{-\alpha\mathcal{L}} \exp\left(-j\frac{\omega_m}{c}\frac{n_{og}+n_e}{2}\mathcal{L}\right) \operatorname{sinc}\left(\frac{\omega_m\mathcal{L}}{2c}(n_{og}-n_e)\right) \tag{72}$$

The above result shows how the modulator bandwidth is limited by the mismatch between the optical group velocity and the electrical phase velocity, i.e. by the difference between the optical group index n_{og} and the electrical phase index n_e. The 3 dB bandwidth is given by

$$f_{3\,\mathrm{dB}} = \frac{1.39\,c}{\pi\mathcal{L}|n_{og}-n_e|} \tag{73}$$

In practical designs, the electrical phase index n_e and optical group index n_{og} can be engineered to minimize the velocity mismatch. For example, a slow-wave electrode design can considerably

Optics EXPRESS

increase n_e, as well as Z_c [16]. Next to the electrode design, silicon modulators can also be optimized by adjusting the junction dopant concentration, which impacts n_e, Z_c, $V_\pi\mathcal{L}$, and α [19], or by modifying the waveguide geometry, which also affects n_{og} [13,15]. Modulators relying on lithium niobate are typically optimized by careful sizing of the electrodes and dielectric layers [23,24].

The group delay of (72) can be calculated as

$$\tau_{gd}(\omega_m) = -\frac{\mathrm{d}}{\mathrm{d}\omega_m} \arg\left(S_{21}^{EOE}(\omega_m)\right) = \frac{n_{og} + n_e}{2}\frac{\mathcal{L}}{c} \tag{74}$$

The modulator has a constant group delay, which is in general a desirable characteristic. The group delay is the average of the group delay of the optical waveguide and the phase delay of the electrical transmission line. Figure 5 shows the S_{21}^{EOE} amplitude response for various lengths $\mathcal{L}$. In this example, $\alpha = 0.5\,\mathrm{dB/mm}$, resulting in a maximum gain length of $\mathcal{L}_{\mathrm{max,\,QP}} \approx 8.7\,\mathrm{mm}$, beyond which the modulator gain no longer increases. A device length of $\mathcal{L} = 4\,\mathrm{mm}$ provides a well-balanced performance, achieving -37.1 dB gain alongside 66.3 GHz bandwidth.

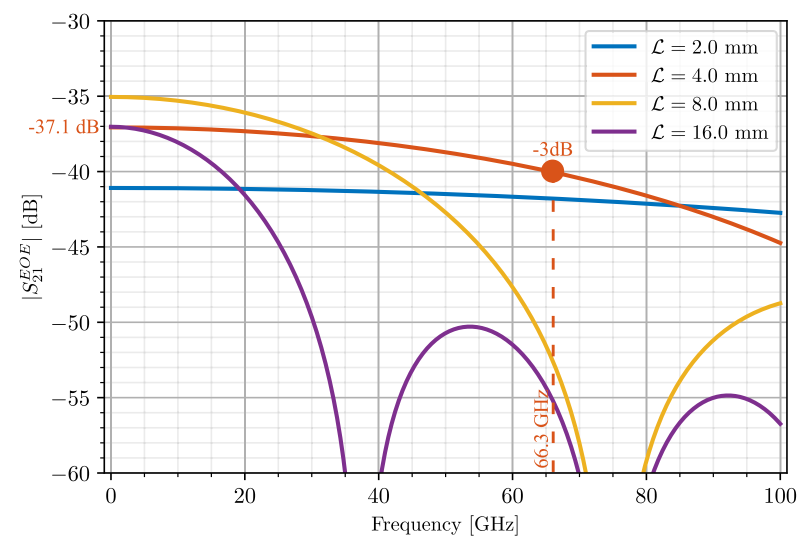

Fig. 5. S_{21}^{EOE} amplitude response for various lengths $\mathcal{L}$. In this numerical example, $R_{01} = 100\,\Omega$, $R_{02} = 50\,\Omega$, $Z_{PD} = R_{02}$, $R = 1\,\mathrm{A/W}$, $P_s = 1\,\mathrm{mW}$, $V_\pi\mathcal{L} = 10\,\mathrm{V\,mm}$, $\alpha = 0.5\,\mathrm{dB/mm}$, $n_{og} = 3.5$ (constant), $n_e = 4$ (constant), $K_S = 0$, $K_T = 0$ and $\alpha_e = 0$.

Transmission line with dispersion. If the transmission line does introduce dispersion, β_e is not a linear function of ω_m, but rather

$$\beta_e(\omega_m) = \frac{\omega_m}{c} n_e(\omega_m) \tag{75}$$

with $n_e(\omega_m)$ the frequency-dependent electrical phase index. Velocity matching is now no longer possible for all frequencies simultaneously, and (66) should be evaluated instead. In general, the group delay of (66) can be written as

$$\tau_{gd}(\omega_m) = \frac{1}{2}\left(\tau + \frac{\mathrm{d}\beta_e}{\mathrm{d}\omega_m}\right)\mathcal{L} \tag{76}$$

$$= \frac{n_{og} + n_{eg}(\omega_m)}{2}\frac{\mathcal{L}}{c} \tag{77}$$

Optics EXPRESS

where $n_{eg}(\omega_m)$ is the frequency-dependent electrical group index. Note that in the dispersionless case, $n_e = n_{eg}$. The modulator group delay is the average of the group delay of the optical waveguide and the group delay of the electrical transmission line.

Although velocity matching is not possible for all frequencies, it might still be possible at a single carrier frequency ω_{m0}, which could be sufficient for some narrowband radio frequency (RF) applications. However, in this special case, should the optical group index n_{og} be matched to the electrical phase index $n_e(\omega_{m0})$ or to the electrical group index $n_{eg}(\omega_{m0})$? To analyze this problem, we can approximate $\beta_e(\omega_m)$ around ω_{m0} as

$$\beta_e(\omega_m) \approx \beta_e(\omega_{m0}) + \left.\frac{\mathrm{d}\beta_e}{\mathrm{d}\omega_m}\right|_{\omega_{m0}} (\omega_m - \omega_{m0}) \tag{78}$$

$$= \frac{\omega_{m0}}{c} n_e(\omega_{m0}) + \frac{n_{eg}(\omega_{m0})}{c}(\omega_m - \omega_{m0}) \tag{79}$$

and use this expression to evaluate (66) around ω_{m0} for different values of $n_e(\omega_{m0})$ and $n_{eg}(\omega_{m0})$. The result is shown in Fig. 6 for $f_{m0} = 30\,\mathrm{GHz}$. If $n_{og} = n_e(\omega_{m0})$, the RF carrier is transferred with maximum efficiency to the optical domain. However, to transfer the RF modulation signal without distortion to the optical domain, a flat response of S_{21}^{EOE} around f_{m0} is required, which requires $n_{og} = n_{eg}(\omega_{m0})$.

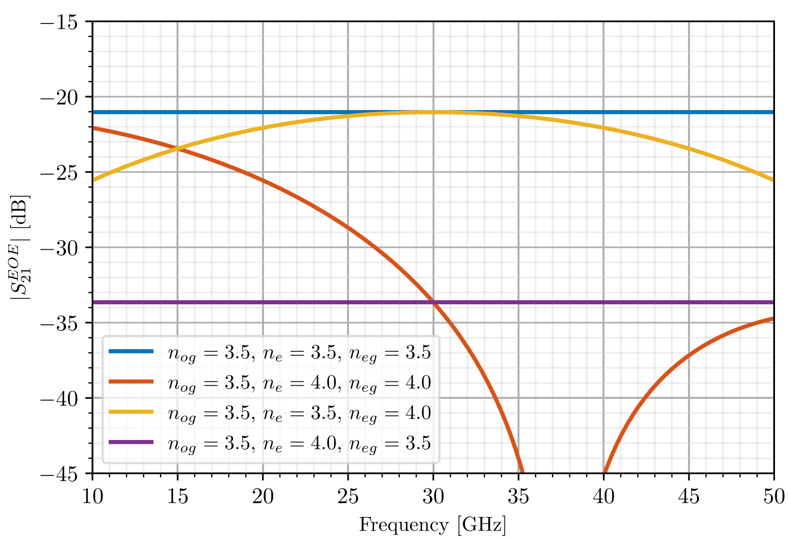

Fig. 6. S_{21}^{EOE} amplitude response around $f_{m0} = 30\,\mathrm{GHz}$ for various values of the electrical indices $n_e(\omega_{m0})$ and $n_{eg}(\omega_{m0})$. In this numerical example, $R_{01} = 100\,\Omega$, $R_{02} = 50\,\Omega$, $Z_{PD} = R_{02}$, $R = 1\,\mathrm{A/W}$, $P_s = 1\,\mathrm{mW}$, $V_\pi \mathcal{L} = 10\,\mathrm{V\,mm}$, $\alpha = 0$, $\mathcal{L} = 16\,\mathrm{mm}$, $K_S = 0$, $K_T = 0$ and $\alpha_e = 0$.

5.2. *Electrical losses*

To isolate the effect of electrical losses, we assume velocity matching has been achieved for all frequencies, i.e.

$$\beta_e = \omega_m \tau \tag{80}$$

In this case, (65) reduces to

$$S_{21}^{EOE}(\omega_m) = \frac{\sqrt{R_{01}R_{02}}}{4} \frac{RP_s\pi}{V_\pi \mathcal{L}} \mathcal{L} e^{-\alpha\mathcal{L}} e^{-j\omega_m\tau\mathcal{L}} \frac{1 - e^{-\alpha_e\mathcal{L}}}{\alpha_e\mathcal{L}} \tag{81}$$

Optics EXPRESS

The 3 dB bandwidth of S_{21}^{EOE} is found for

$$\alpha_e(2\pi f_{3\,\mathrm{dB}})\,\mathcal{L} = 0.738 \tag{82}$$

This corresponds to the −6.4 dB point of the voltage transfer function (53):

$$20\log_{10}\left|\frac{V_d(\mathcal{L})}{V_d(0)}\right| = 20\log_{10} e^{-0.738} \approx -6.4\,\mathrm{dB} \tag{83}$$

If the modulation bandwidth is limited by the electrical losses on the transmission line, the 3 dB EOE bandwidth can be estimated from the −6.4 dB point of the voltage transfer function over the transmission line (53). This relationship is illustrated in Fig. 7, where it was assumed the electrical attenuation α_e is dominated by skin effect, and therefore increases as $\sqrt{f_m}$ [23]. Since the electrical response (53) is typically easier to measure and more accessible than the EOE response (81), this result is of significant practical importance.

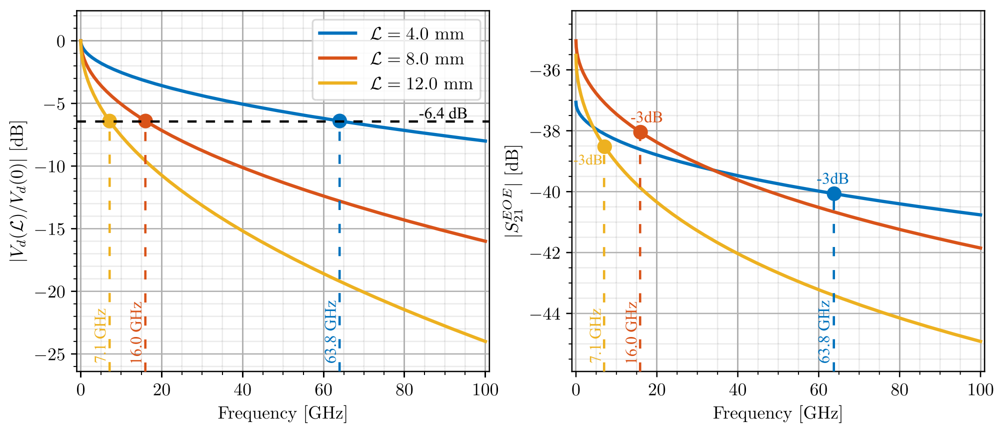

Fig. 7. Voltage transfer function $|V_d(\mathcal{L})/V_d(0)|$ and S_{21}^{EOE} amplitude response for various lengths $\mathcal{L}$. The corresponding −6.4 dB and −3 dB points are indicated by the dots. In this numerical example, $R_{01} = 100\,\Omega$, $R_{02} = 50\,\Omega$, $Z_{PD} = R_{02}$, $R = 1\,\mathrm{A/W}$, $P_s = 1\,\mathrm{mW}$, $V_\pi\mathcal{L} = 10\,\mathrm{V\,mm}$, $\alpha = 0.5\,\mathrm{dB/mm}$, $n_{og} = 4$ (constant), $n_e = 4$ (constant), $K_S = 0$, $K_T = 0$ and $\alpha_e(2\pi\,100\,\mathrm{GHz}) = 2\,\mathrm{dB/mm}$.

From (81) it is readily observed that the modulator group delay τ_{gd} is constant and given by

$$\tau_{gd} = \tau\mathcal{L} = n_{og}\frac{\mathcal{L}}{c} = n_e\frac{\mathcal{L}}{c} \tag{84}$$

In [23], the authors report a 5 mm-long, 50 Ω thin-film lithium niobate (TFLN) MZM that achieves near-perfect velocity matching, with $n_e = 2.21$ and $n_{og} = 2.24$. Measurements indicate that the electrical attenuation α_e scales with $\sqrt{f_m}$, showing a loss of about 1.0 dB/mm at 100 GHz. Using these parameters in (81) yields a reduction of S_{21}^{EOE} by 2.49 dB at 110 GHz, which closely matches the 2.5 dB reduction observed experimentally in [23].

5.3. Impedance mismatch

If the termination resistor R_T is not matched to the transmission line characteristic impedance Z_c, $K_T \neq 0$, and the voltage distribution $V_d(z)$ now also contains a component traveling in the $-z$-direction, opposite to the direction of light propagation. To analyze the influence of this counter-propagating wave on S_{21}^{EOE}, we start from (59), choose $Z_{PD} = R_{02}$, neglect the electrical

Optics EXPRESS

attenuation ($\alpha_e = 0$), and further assume the transmission line is dispersionless (see (70)). This leads to

$$S_{21}^{EOE}(\omega_m) = \frac{\sqrt{R_{01}R_{02}}}{2}\frac{RP_s\pi}{V_\pi\mathcal{L}}\mathcal{L}e^{-\alpha\mathcal{L}}A^+(\omega_m)\exp\left(-j\frac{\omega_m}{c}\frac{n_{og}+n_e}{2}\mathcal{L}\right) \left[\underbrace{\operatorname{sinc}\left(\frac{\omega_m\mathcal{L}}{2c}(n_{og}-n_e)\right)}_{\text{slow roll-off}} + K_T\exp\left(-j\frac{\omega_m}{c}n_e\mathcal{L}\right)\underbrace{\operatorname{sinc}\left(\frac{\omega_m\mathcal{L}}{2c}(n_{og}+n_e)\right)}_{\text{fast roll-off}}\right] \quad (85)$$

For $K_T = K_S = 0$, this result reduces to (72). The presence of the factor $A^+(\omega_m)$, given by (51), will lead to ripple in the modulator frequency response for $K_S \neq 0$, which is generally undesirable. The co-propagating and counter-propagating waves each give rise to a sinc$(\cdot)$ term, with the latter having a much faster roll-off due to the inherent velocity mismatch between waves traveling in opposite directions. This effect can be used to alter the gain at low frequencies, while leaving the high-frequency response untouched. Of particular interest is the case $K_T<0$, which reduces the low-frequency gain and therefore increases the modulator bandwidth. It is easily shown that for $K_S = 0$ and $n_{og} \approx n_e$, $K_T \neq 0$ introduces a low-frequency change in amplitude of

$$\Delta S_{21}^{EOE}(0)\ [\mathrm{dB}] = 20\log_{10}(1+K_T) \quad (86)$$

$$= 20\log_{10}\left(\frac{2R_T}{R_T+Z_c}\right) \quad (87)$$

with the amplitude response being restored to its nominal value around

$$f_{0\,\mathrm{dB}} = \frac{c}{2(n_{og}+n_e)\mathcal{L}} \quad (88)$$

Figure 8 shows the S_{21}^{EOE} amplitude response and group delay for various values of K_S and K_T, in the presence of limited velocity mismatch. For the cases with $K_S = 0$, $\Delta S_{21}^{EOE}(0) \approx -2.5$ dB for $K_T = -0.25$ and $\Delta S_{21}^{EOE}(0) \approx 1.9$ dB for $K_T = 0.25$, with $f_{0\,\mathrm{dB}} = 5$ GHz. It is worth noting that the presence of the counter-propagating wave leads to large variations in the modulator group delay (a variation of 25.5 ps from 32.2 ps to 57.7 ps for the device with $K_S = 0$ and $K_T = -0.25$), which is generally undesirable and causes linear distortion.

5.4. Combining velocity mismatch, electrical losses and impedance mismatch

To combine all of the above effects, we return to the original expression of S_{21}^{EOE} and evaluate (59) numerically. Figure 9 shows the result for a select few cases. As expected, the longer modulator with $\mathcal{L} = 4$ mm has more gain and a faster roll-off than the 2 mm device. The fast roll-off at low frequencies (due to skin effect) can be partially compensated by choosing $K_T<0$, at the cost of low-frequency gain and ripple in the amplitude response and group delay (4.1 ps variation for the 2 mm device and 8.0 ps variation for the 4 mm device). The combined effect of velocity mismatch and electrical losses results in a 3 dB bandwidth of approximately 34.5 GHz for the device with $\mathcal{L} = 4$ mm and $K_T = 0$, compared to 66.3 GHz for the case with only velocity mismatch (Fig. 5) or 63.8 GHz for the case with only electrical losses (Fig. 7).

To confirm the validity of the presented model, we compare it against existing models for the parameters of the purple curve ($\mathcal{L} = 4.0$ mm and $K_T = -0.1$) from Fig. 9. Table 1 presents an overview. All models predict the same amplitude frequency response after normalization, but only this work discusses modulator gain by carefully defining S_{21}^{EOE}. In addition, phase response and group delay, which are important system characteristics, are discussed in detail.

Optics EXPRESS

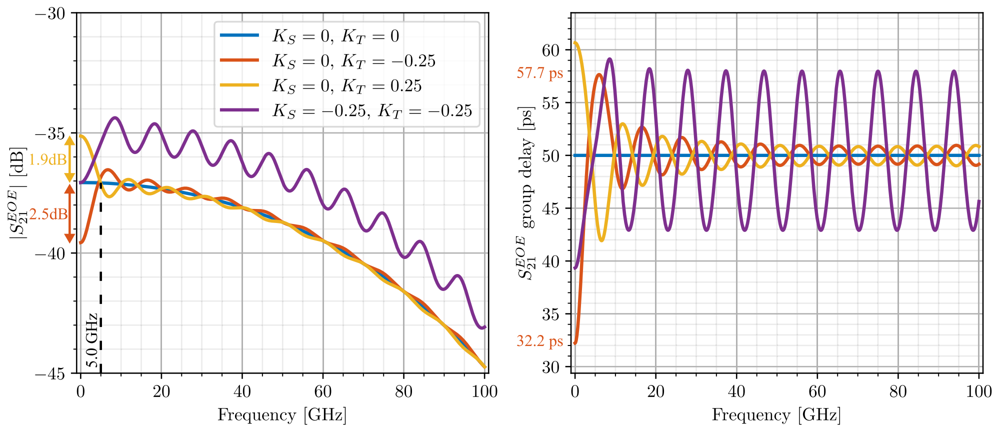

Fig. 8. S_{21}^{EOE} amplitude response and group delay for various cases of impedance mismatch. In this numerical example, $R_{01} = 100\,\Omega$, $R_{02} = 50\,\Omega$, $Z_{PD} = R_{02}$, $R = 1\,\mathrm{A/W}$, $P_s = 1\,\mathrm{mW}$, $V_\pi \mathcal{L} = 10\,\mathrm{V\,mm}$, $\alpha = 0.5\,\mathrm{dB/mm}$, $\mathcal{L} = 4\,\mathrm{mm}$, $n_{og} = 3.5$ (constant), $n_e = 4$ (constant) and $\alpha_e = 0$.

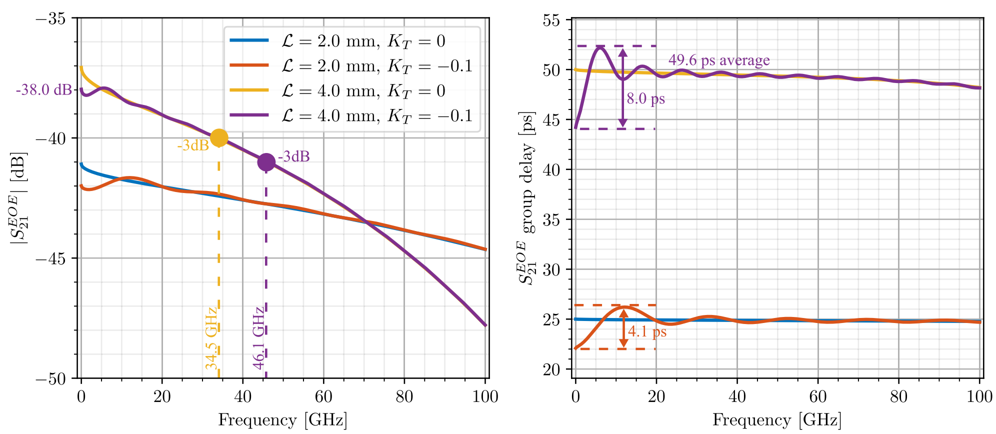

Fig. 9. S_{21}^{EOE} amplitude response and group delay for various lengths $\mathcal{L}$ and termination resistors R_T. In this numerical example, $R_{01} = 100\,\Omega$, $R_{02} = 50\,\Omega$, $Z_{PD} = R_{02}$, $R = 1\,\mathrm{A/W}$, $P_s = 1\,\mathrm{mW}$, $V_\pi \mathcal{L} = 10\,\mathrm{V\,mm}$, $\alpha = 0.5\,\mathrm{dB/mm}$, $n_{og} = 3.5$ (constant), $n_e = 4$ (constant), $K_S = 0$ and $\alpha_e(2\pi\,100\,\mathrm{GHz}) = 2\,\mathrm{dB/mm}$.

Table 1. Comparison between the presented model and existing models for the same parameter set as the purple curve ($\mathcal{L} = 4.0\,\mathrm{mm}$, $K_T = -0.1$) in Fig. 9.

	3 dB bandwidth	Gain	Average group delay over bandwidth	Group delay variation over bandwidth
This work	46.1 GHz	-38.0 dB	49.6 ps	8.0 ps
[3]	46.1 GHz	Normalized	Not discussed	Not discussed
[6]	46.1 GHz	Normalized	Not discussed	Not discussed

6. Minimum transmission point biasing

Another way to obtain a linear EOE channel is by biasing the modulator in its MTP and using a homodyne coherent receiver. If we revisit (24) and choose $\phi_B = \pi$, again with $v_U(z,t) = -v_L(z,t) = \frac{1}{2}\, v_d(z,t)$, we find

$$e_{out}(t) = -j \sin\left\{\frac{\pi}{2V_\pi \mathcal{L}} \int_0^{\mathcal{L}} v_d(z, t + \tau(z - \mathcal{L}))\, \mathrm{d}z\right\} e^{-\frac{\alpha}{2}\mathcal{L}}\, e^{-j\frac{2\pi}{\lambda_0} n_0 \mathcal{L}}\, e_{in}(t - \tau\mathcal{L}) \tag{89}$$

As this equation shows, only a single quadrature is being modulated. To cover the full IQ-plane, a second MZM would be required. To detect a single quadrature of the optical field $e_{out}(t)$, we can use a simplified homodyne receiver, as shown in Fig. 10.

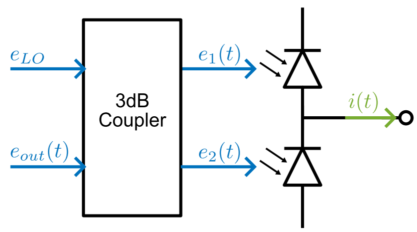

Fig. 10. Single-quadrant coherent receiver.

The local oscillator (LO) frequency is assumed to be perfectly matched to the carrier frequency f_0 (homodyne detection), and its phase can be arbitrarily set to j, such that

$$e_{LO} = j\sqrt{P_{LO}} \tag{90}$$

The optical fields impinging on the photodetectors are given by

$$e_1(t) = \frac{1}{\sqrt{2}}\,(e_{LO} + je_{out}(t)) \tag{91}$$

$$e_2(t) = \frac{1}{\sqrt{2}}\,(je_{LO} + e_{out}(t)) \tag{92}$$

From this, the current $i(t)$ can be derived as

$$i(t) = R\,(|e_1(t)|^2 - |e_2(t)|^2) \tag{93}$$

$$= 2R\,\Im\{e_{LO}\, e^*_{out}(t)\} \tag{94}$$

To simplify the results, we arbitrarily choose the phase of the transmitter laser source such that $e_{in}(t) = j\, e^{j\frac{2\pi}{\lambda_0} n_0 \mathcal{L}}\, \sqrt{P_s}$. The current $i(t)$ now becomes

$$i(t) = 2R\sqrt{P_{LO}P_s}\, e^{-\frac{\alpha}{2}\mathcal{L}} \sin\left\{\frac{\pi}{2V_\pi \mathcal{L}} \int_0^{\mathcal{L}} v_d(z, t + \tau(z - \mathcal{L}))\, \mathrm{d}z\right\} \tag{95}$$

For a small-signal approximation, this result can be linearized around $v_d = 0$ for $|v_d| \ll V_\pi$. Using $\sin(x) \approx x$, we get

$$i(t) \approx \frac{R\sqrt{P_{LO}P_s}\,\pi}{V_\pi \mathcal{L}}\, e^{-\frac{\alpha}{2}\mathcal{L}} \int_0^{\mathcal{L}} v_d(z, t + \tau(z - \mathcal{L}))\, \mathrm{d}z \tag{96}$$

Comparing the signal part $\Delta i(t)$ of (29) with (96), it can be concluded that both results are the same after replacing the factor $P_s e^{-\alpha\mathcal{L}}$ by $2\sqrt{P_{LO}P_s}e^{-\frac{\alpha}{2}\mathcal{L}}$ in (96). As a result, also the EOE transfer function (33) is still valid after making the same adjustments:

$$I = \frac{R\sqrt{P_{LO}P_s}\pi}{V_\pi \mathcal{L}} \, e^{-\frac{\alpha}{2}\mathcal{L}} \, e^{-j\omega_m \tau \mathcal{L}} \int_0^{\mathcal{L}} V_d(z) \, e^{j\omega_m \tau z} \, \mathrm{d}z \tag{97}$$

In this case however, the maximum modulator gain is found for

$$\mathcal{L}_{\text{max, MTP}} = \frac{2}{\alpha} \tag{98}$$

For coherent modulation, the modulator can be made twice as long as compared to intensity modulation, before optical losses start to dominate any improvement in V_π. Because the transfer functions (33) and (97) share the same frequency dependence, both EOE channels have the same 3 dB modulation bandwidth.

The PSD $S_{out}(f)$ of the modulated optical field in the case of MTP biasing is given by

$$S_{out}(f) = \frac{P_s \pi^2}{16(V_\pi \mathcal{L})^2} e^{-\alpha\mathcal{L}} \left| \int_0^{\mathcal{L}} V_d(z) \, e^{j\omega_m \tau z} \, \mathrm{d}z \right|^2 (\delta(f - f_m) + \delta(f + f_m)) \tag{99}$$

from which $\hat{S}_{out}(f)$ can be found using (42). Comparing this result with (41), the frequency component at f_0 has disappeared, and only the components at $f_0 \pm f_m$ remain.

7. Conclusion

A rigorous small-signal system-level analysis of traveling-wave Mach-Zehnder modulators was presented. It was shown how an EOE transfer function can be formally derived, and special attention was paid to the existence of different definitions for the 3 dB modulation bandwidth. EOE S-parameters were introduced to analyze the gain and bandwidth of a TWMZM, and the effects of velocity mismatch, impedance mismatch, and electrical losses were examined in detail. In particular, the importance of dispersion on the electrical transmission line in relation to velocity matching, and the corresponding electrical phase and group indices, was discussed. Finally, the analysis was extended to coherent systems relying on minimum transmission point biasing.

Optics EXPRESS

Appendix

Table 2 presents an overview of key symbols and their units.

Table 2. Key symbols and their units.

Symbol	Unit	Description
α	m^{-1}	optical attenuation coefficient
α_e	m^{-1}	electrical loss coefficient
β	m^{-1}	optical propagation factor
β_e	m^{-1}	electrical propagation factor
γ_e	m^{-1}	complex electrical propagation factor
τ	s/m	optical group delay per unit length
f_0	Hz	optical center frequency
f_m	Hz	modulation frequency
f_{m0}	Hz	RF carrier frequency
K_S		source reflection coefficient
K_T		termination reflection coefficient
$\mathcal{L}$	m	modulator length
n_e		electrical phase index
n_{eg}		electrical group index
n_0		optical effective phase index
n_{og}		optical group index
P_s	W	laser launch power
R	A/W	photodetector responsivity
R_{01}	Ω	source output resistance
R_{02}	Ω	loading of subsequent receiver circuits
R_T	Ω	termination resistor
$V_\pi \mathcal{L}$	V m	phase shifter efficiency
Z_c	Ω	transmission line characteristic impedance
Z_{PD}	Ω	photodetector output impedance

Funding. Research Foundation - Flanders (1SB7720N, 1SB7722N).

Acknowledgment. The authors would like to thank Jonas De Busscher, Aboobackkar Sidhique and Simone Cammarata for checking the equations and proofreading the text.

Disclosures. The authors declare no conflicts of interest.

Data availability. Data underlying the results presented in this paper are not publicly available at this time but may be obtained from the authors upon reasonable request.

References

1. I. P. Kaminow, "Microwave Modulation of the Electro-Optic Effect in KH_2PO_4," Phys. Rev. Lett. **6**(10), 528–530 (1961).
2. W. W. Rigrod and I. P. Kaminow, "Wide-Band Microwave Light Modulation," Proc. IEEE **51**(1), 137–140 (1963).
3. G. Ghione, *Semiconductor Devices for High-Speed Optoelectronics* (Cambridge University, 2009).
4. K. Kubota, J. Noda, and O. Mikami, "Traveling Wave Optical Modulator Using a Directional Coupler LiNbO3 Waveguide," IEEE J. Quantum Electron. **16**(7), 754–760 (1980).
5. H. Yu and W. Bogaerts, "An Equivalent Circuit Model of the Traveling Wave Electrode for Carrier-Depletion-Based Silicon Optical Modulators," J. Lightwave Technol. **30**(11), 1602–1609 (2012).
6. S. H. Lin and S.-Y. Wang, "High-throughput GaAs PIN electrooptic modulator with a 3-dB bandwidth of 9.6 GHz at 1.3 μm," Appl. Opt. **26**(9), 1696–1700 (1987).

Optics EXPRESS

7. R. C. Alferness, "Waveguide Electrooptic Modulators," IEEE Trans. Microwave Theory Tech. **30**(8), 1121–1137 (1982).
8. H. Xu, X. Li, X. Xiao, *et al.*, "Demonstration and Characterization of High-Speed Silicon Depletion-Mode Mach–Zehnder Modulators," IEEE J. Sel. Top. Quantum Electron. **20**(4), 23–32 (2014).
9. A. Yariv, *Introduction to Optical Electronics* (Holt, Rinehart & Winston, 1976), 2nd ed.
10. Keysight Technologies, "High Speed Lightwave Component Analysis - Application Note," (2017). https://www.keysight.com/us/en/assets/7018-01732/application-notes/5989%-7808.pdf.
11. G. P. Agrawal, *Fiber-Optic Communication Systems* (John Wiley & Sons, Inc., 2010), 4th ed.
12. J. Wang and K. Petermann, "Small Signal Analysis for Dispersive Optical Fiber Communication Systems," J. Lightwave Technol. **10**(1), 96–100 (1992).
13. E. Dulkeith, F. Xia, L. Schares, *et al.*, "Group index and group velocity dispersion in silicon-on-insulator photonic wires," Opt. Express **14**(9), 3853–3863 (2006).
14. Y. He, H. Liang, R. Luo, *et al.*, "Dispersion engineered high quality lithium niobate microring resonators," Opt. Express **26**(13), 16315–16322 (2018).
15. R. H. Khandokar, M. Bakaul, S. Skafidas, *et al.*, "Performance of Planar, Rib, and Photonic Crystal Silicon Waveguides in Tailoring Group-Velocity Dispersion and Mode Loss," IEEE J. Sel. Top. Quantum Electron. **22**(2), 73–80 (2016).
16. R. Ding, Y. Liu, Y. Ma, *et al.*, "High-Speed Silicon Modulator With Slow-Wave Electrodes and Fully Independent Differential Drive," J. Lightwave Technol. **32**(12), 2240–2247 (2014).
17. L. Breyne, J. Lambrecht, M. Verplaetse, *et al.*, "Electro-Optic Frequency Response Shaping using Embedded FIR Filters in Slow-Wave Modulators," J. Lightwave Technol. **39**(6), 1777–1784 (2021).
18. A. Wissing, J. Dalton, E. Chansky, *et al.*, "A Monolithically Integrated Five-Segment Mach–Zehnder Modulator With Distributed Driver in 45-nm CMOS," IEEE Photonics Technol. Lett. **38**(4), 251–254 (2026).
19. J. Witzens, "High-Speed Silicon Photonics Modulators," Proc. IEEE **106**(12), 2158–2182 (2018).
20. R. G. Walker, "High-Speed III-V Semiconductor Intensity Modulators," IEEE J. Quantum Electron. **27**(3), 654–667 (1991).
21. X. Chen, S. Chandrasekhar, G. Raybon, *et al.*, "Characterization of Electro-Optic Bandwidth of Ultra-High Speed Modulators," in *Optical Fiber Communication Conference*, (Optica Publishing Group, 2017), p. Tu2H.7.
22. D. M. Pozar, *Microwave Engineering* (John Wiley & Sons, Inc., 2012), 4th ed.
23. X. Fang, F. Yang, X. Chen, *et al.*, "Ultrahigh-Speed Optical Interconnects With Thin Film Lithium Niobate Modulator," J. Lightwave Technol. **41**(4), 1207–1215 (2023).
24. M. Zhang, C. Wang, P. Kharel, *et al.*, "Integrated lithium niobate electro-optic modulators: when performance meets scalability," Optica **8**(5), 652–667 (2021).